# Effect of surface preparation on oxidation of austenitic SS 304L in high temperature water

**Annesha DAS[1], Supratik ROYCHOWDHURY[2], Vivekanand KAIN[3]**

*[1]Homi Bhabha National Institute, Mumbai, India, anneshad@barc.gov.in*
*[2]Materials Processing & Corrosion Engineering Division, Bhabha Atomic Research Centre, Mumbai, India, supratik@barc.gov.in*
*[3]Materials Processing & Corrosion Engineering Division, Bhabha Atomic Research Centre, Mumbai, India, vivkain@barc.gov.in*

Abstract

Oxide passive film formed on austenitic stainless steel exposed to high temperature high pressure (HTHP) water simulating light water reactor (LWR) conditions have been widely investigated for their electronic properties, morphology and chemical composition. The effects of surface finishing operations (machining, milling, grinding, electropolishing, mechanical grinding by emery paper and diamond polishing) on these oxides formed in different HTHP water chemistries have been characterised for differences in oxide film thickness, chromium content and film resistance (to breakdown) due to difference in surface and sub-surface deformations developed as a result of these operations. The nature of oxides formed on surface machined specimens in HTHP water have been reported to be either protective (higher chromium content in inner layer due to enhanced chromium diffusion possibly making it more impervious and protective) or non-protective (nonuniform, porous and thick oxides over machined surfaces anticipated to facilitate rupture under stress). Chromium enrichment in oxides was reported to have formed over electropolished surfaces, thus forming a better protective oxide. Thus, a consensus over the effect of surface working on the protective nature of the oxide formed in HTHP water on austenitic stainless steel is lacking. Also, few studies have compared effect of surface working during long term HTHP water exposures on the oxide film development and its properties.

In the present work, plates of SS 304L were machined and the surface/subsurface changes were characterized by optical and scanning electron microscopy (SEM), 3D-optical profilometry, microhardness and electron back scattered diffraction (EBSD) techniques. Machining grooves were shown to be ~ 100 µm apart. Preliminary cross-sectional EBSD showed a severely plastically deformed (SPD) surface region due to machining, followed by a strained subsurface region of thicknesses ~15 µm and ~ 90 µm respectively. The corresponding high hardness values were also established i.e. ~444 $HV_{10}$ at the surface whereas bulk hardness is ~252 $HV_{10}$. The growth kinetics of the oxide layer on machined coupons was studied after exposure to demineralised water at 300 ˚C and 89 bar in a static autoclave with DO <5 ppb for 15, 30, 45 and 60 days. Oxides formed on machined, electropolished, diamond polished and #600 mechanically polished coupons - exposed to similar water chemistry for 15 days – were studied. The morphology of oxides formed were characterised along with the weight change after exposure. Glow – discharge optical emission spectroscopy (GDOES) was used for elemental depth profiling in the oxides. The SEM images showed a decrease in number of outer oxide particles with increase in oxidation time. A weight loss was recorded as a result of oxidation of machined coupons for all the exposure durations up to 60 days. Further results are discussed in detail.

Keywords: surface film, high temperature water, machining, oxides

## Introduction

Austenitic stainless steels are an important class of metals used as construction material in nuclear power plants (NPPs) for their high corrosion resistant and toughness. However, environmentally assisted degradation mechanisms like stress corrosion cracking (SCC) significantly reduce their dependability [1-7]. SCC initiation is a stochastic process that depends largely on the material surface condition, which in turn, is affected by surface finishing operations – an unavoidable part of the component fabrication process. Surface finishing processes viz. machining, grinding, turning, milling, etc. severely affect the initiation process by introducing changes in the surface and subsurface layers of the metal viz. change in surface roughness, grain fragmentation, conversion of austenite to strain-induced martensite and introduction of residual stresses [8-15]. Change in surface reactivity [16] changes the behavior of the passive films formed over the surface. Researchers have investigated passive films formed over surface worked specimens formed during exposure to different environments [13-21]. While some have resulted a beneficial effect of surface working on the stability of the passive film viz. an increase in chromium concentration leading to a more protective film [17], others have reported that surface working resulted in non-uniform films with lowered chromium content [18] that "debonded" easily from the oxide/substrate interface [13-15]. However, these studies have only compared different surface states resulting from different surface operations exposed to the environment for a given duration of time. To the best of the knowledge of the authors, a systematic study of the long term oxide development over surface worked SS specimens has not been reported in open literature.

The present work is a part of a larger study that aims to establish the developmental behavior of oxides formed over machined SS304L exposed to high temperature DM water for up to 60 days. To compare the differences in morphology of oxides formed over different surface states, coupons of #600 grit emery paper polished, diamond polished and electropolished specimen were exposed to high temperature DM water for 15 days.

## Experimental Procedures

### Base Material

A SS304L plate of following composition (as determined by Inductively Coupled Plasma-Optical Emission Spectroscopy (ICP-OES)) was used for the present study: 17.70 ± 0.22 Cr, 9.12 ± 0.17 Ni, 0.019 ± 0.002 C, 1.65 ± 0.02 Mn, 0.35 ± 0.01 Cu, 0.14 ± 0.01 Mo, 0.40 ± 0.01 Si, 0.04 ± 0.003 P, 0.007 N, 0.0038 ± 0.00001 S, balance Fe (all in wt.%). The as-received (AR) plate was cut into coupons of 10 mm x 10 mm x 3 mm which were then metallographically ground on successively finer SiC papers up to #1200 grit and finally diamond paste (1 μm). Average Vickers microhardness, measured from 10 readings taken on the polished AR surface using a diamond indenter at a load of 300 gf and a dwell time of 20 s, was reported along with standard error. Ferrite content was measured using a ferritemeter. Polished specimens were electrolytically etched in 10 % oxalic acid at a current density of 1 $A/cm^2$ for a period of 90 s [22] for microstructural examination under an optical microscope. Grain size was calculated using the linear intercept method [23] using over 300 readings from at least 10 images.

### Machining and subsequent characterisation

A SS304L plate of 150 mm x 150 mm x 3 mm was machined by a carbide tool at 200 rpm and 0.125 mm/min feed rate using a centre lathe machine to remove 0.5 mm from both sides of the plate.

The topography of the machined plates was characterised using a field emission-scanning electron microscope (FE-SEM). A non-contact, interferometry-based 3D-optical profilometer was used to measure the surface average roughness ($S_a$) of the machined surface. At least ten readings were taken across the machined plate surface and the range was reported.

Cross sections of machined specimens were hot mounted metallographically polished and subsequently electroetched [22] for scanning electron microscopy. EBSD was used to map the misorientations introduced due to machining as a qualitative representation of the residual strains causing lattice deformations within the grains. For EBSD, metallographically prepared polished cross-sections samples of machined SS304L were further colloidal polished using colloidal silica (0.04 μm finish) to remove the surface layer affected by colloidal polishing. An FE-SEM equipped with optical imaging microscopy (OIM) system was used at an operating voltage of 20 kV with a 60 μm aperture. Beam step size was kept at 0.1 μm and a confidence index (CI) of 0.1 was used. Scans were taken just beneath the surface to distinguish between the mount and highly deformed surface layers. 10 different scans were taken at different regions. Extent of deformation was qualitatively examined by using kernel average misorientation (KAM) maps which give crystal lattice misorientations (indicative of strain) in a pixel compared to the average orientation of the neighbouring pixels.

While direct measurement of the residual strains induced due to machining were not done, the gradual change in extent of deformation from the surface down to the bulk was characterised by cross-sectional hardness measurement and electron backscattered microscopy (EBSD). Colloidal polished (0.04 μm finish) cross-sections were oriented 45º to the vertical and hardness measurements were done using an instrumented hardness tester equipped with a diamond indenter. A load of 10 gf was used with a loading time of 20 s, holding time of 5 s and unloading time of 20 s. A low load and 45º angle to the vertical ensured more number of data points within the deformed zone. 25 readings were taken and plotted to show the variation in hardness with depth. The distance from the machined edge to the mid-point of the indent was taken as the depth corresponding to that hardness value. As indent diagonal was roughly 10 μm, the values very near the surface could not be obtained. 10 measurements were taken at the mid-thickness of the machined cross-section and the average hardness value was compared with that at the mid-thickness of the AR sample to show that there was no change. Average mid-thickness hardness value along with standard error based on 10 readings were plotted.

<u>High temperature exposure</u>

Exposure coupons were cut out from the AR and machined sheets and prepared for exposure to high temperature water by relevant mechanical grinding and polishing techniques. Dimensions of each coupon were measured using a Vernier calliper (least count 0.01 mm) to calculate areas of exposure. All cross-sections were polished using successively finer emery paper till #600 grit. Contribution of these surfaces were assumed to be same for all exposure conditions and error introduced as a result was assumed to be same for all. Coupons were thoroughly cleaned using soap solution and acetone to remove any grease on the surface and dried properly. Pre-exposure weights ($W_1$) were taken as the average of 6 measurements for each sample using a weighing balance with least count of 1 μm.

Two sets of experiments were carried out.

I. In the first set, changes in oxides formed over machined surfaces during prolonged exposure times were investigated by immersing 16 coupons of machined SS304L (25 mm × 25 mm × 2 mm) in the autoclave for 15, 30, 45 and 60 days. All coupons were exposed simultaneously to ensure similar exposure conditions and 4 samples were taken out every 15 days as a sub-set. The autoclave was filled with fresh DM water at

this juncture before re-immersing the rest of the samples. This was done to avoid ionic saturation of the exposure environment.

II. In the second set of experiments, coupons with machined, electropolished, diamond polished (0.25 microns) and #600 grit finished surfaces were exposed to high temperature water in order to study the influence of surface condition on oxides formed. Coupons were of nominal dimensions 25 mm × 25 mm × 3 mm (thickness), except for the machined coupons which had a thickness of 2 mm. A solution of 80:20 methanol : perchloric acid was used to electropolish the coupons. 4 coupons of each surface condition were taken and all 16 were simultaneously exposed to DM water at 300 °C and 89 bar for 15 days.

The nomenclature of all samples exposed is detailed in Table 1.

| Test Set | Sample Condition | Duration of exposure (days) | Sample designation |
|---|---|---|---|
| I | Machined | 15 | M15 |
| I | Machined | 30 | M30 |
| I | Machined | 45 | M45 |
| I | Machined | 60 | M60 |
| II | Machined | 15 | MC |
| II | #600 grit polished | 15 | 600 |
| II | Diamond polished | 15 | DP |
| II | Electropolished | 15 | MP |

***Table 1: Identification of coupons for high temperature oxidation based on surface finish and exposure durations.***

High temperature oxidation studies were carried out in a 1.5 L static autoclave made of SS316. The test temperature and pressure were maintained at 300 °C and 89 bar, respectively. 940 ml (calculated from ASTM G2M) of demineralised water was used with DO < 5 ppb. Deaeration was achieved by purging the autoclave with high purity nitrogen gas during heating (up to 70 ˚C) and subsequently venting at 150 ˚C. No hydrogen was added in this study. At the end of the test, the autoclave was allowed to cool down to room temperature before taking out the samples. Oxidised coupons were then washed carefully using deionized water and dried before weighing (as explained above). This weight was denoted as $W_2$. They were then ultrasonicated for 2 min (1 min each in acetone and DM water) and dried before having their weights taken again. This weight was denoted as $W_{2U}$ (weight after ultrasonic cleaning). The specific weight change due to high temperature oxidation was then calculated as per equ. (1):

$$\text{Sp. wt. change (w)} = \frac{W_{\text{pre-exposure}} - W_{\text{post-exposure}}}{A} \qquad (1)$$

where,

$W_{\text{pre-exposure}}$ is $W_1$

$W_{\text{post-exposure}}$ is $W_2$ for without and $W_{2U}$ for with ultrasonic cleaning.

A is the area of exposure including the cross-sections.

Oxide Characterisation

The dried coupons were imaged using a stereomicroscope to check the uniformity of oxide coverage. Oxide morphologies were examined before and after ultrasonic cleaning using FE-SEM at 20kV with a 20 μm aperture. The outer oxide particle sizes were calculated for every

condition of test set I and II using ImageJ and at least 5 images at 30,000x and plotted. Change in specific weights of the oxidised coupons with and without ultrasonic cleaning for both test sets I and II were also plotted individually. To show the change in elemental concentration at the inner/outer oxide interface, elemental depth profiling was carried out using glow discharge – optical emission spectroscopy.

## Results

As-received SS304L

Fig 1 shows the etched microstructure of AR SS304L. The average grain size measured from microstructure was 35 ± 2 µm, microhardness was 165 ± 8 $HV_{300}$ and the ferrite content was < 0.2% (i.e. below detection limit of the instrument).

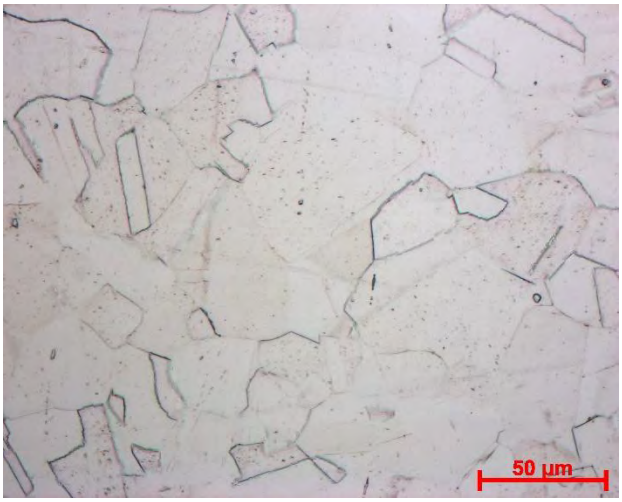


***Fig 1. Microstructure of etched SS304L***

Machined SS304L

Pre-exposure characterisation:

Fig 2 shows a representative SEM image of the machined surface Machining resulted in a surface with periodic striations approximately 100 µm apart. Regular machining grooves along with surface artefacts viz. smear/adhesive chips, microcracks and microcavities were observed on the surface. This type of topography is characteristic of a machined surface and has been previously reported [28]. The $S_a$ value ranged between 1.2 – 1.6 µm, higher than that for the AR surface (0.3 – 0.6 µm).

Fig 3 and Fig 4 present representative SEM and EBSD images showing the cross-sectional microstructure of machined SS304L. In the SEM image (Fig. 3), a heavily damaged top layer is visible post machining with unidentifiable grain structure. This region with nano/ultrafine grains is called the severely plastically deformed (SPD) layer and is identified as the high strain region in the KAM (Fig. 4) maps marked in red and delineated by white dotted line. Misorientation angles are very high in this region (as shown by the colour index) and are indicative of heavy strains resulting as a consequence of machining. The region just beneath the SPD layer is marked by identifiable grain structure with misorientations (green zones) concentrated both within (towards the top) and at the grain boundaries (at a greater distance from the surface). Grain structure is now present, with a heavy amount of straining within the grains. This region is termed as the deformed sub-surface region and is not as visible in the SEM images as in the KAM maps. While etching the samples for SEM, prolonged application

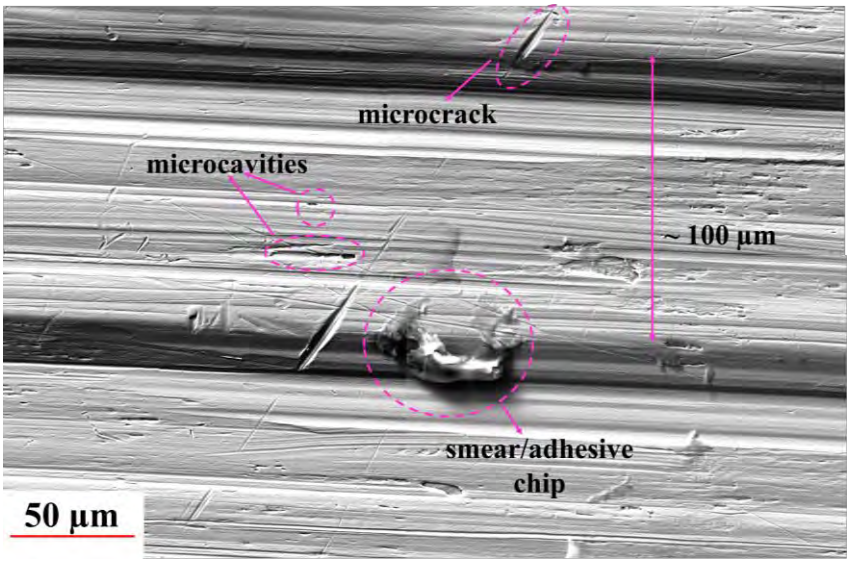


***Fig 2. SEM image of machined surface, showing machining tracks and surface artefacts.***

of voltage caused the top SPD layer to disappear. A strain free blue matrix with minimum misorientation (and hence, strain) is observed beneath this region which is the bulk. Thicknesses of each individual layer was measured at 10 – 15 equidistant points on the ten SEM and EBSD images taken. The layers varied non-uniformly. The SPD layer varied up to 10 µm from the top machined surface. The sub-surface deformed layer extended a further 100 µm deeper into the matrix.

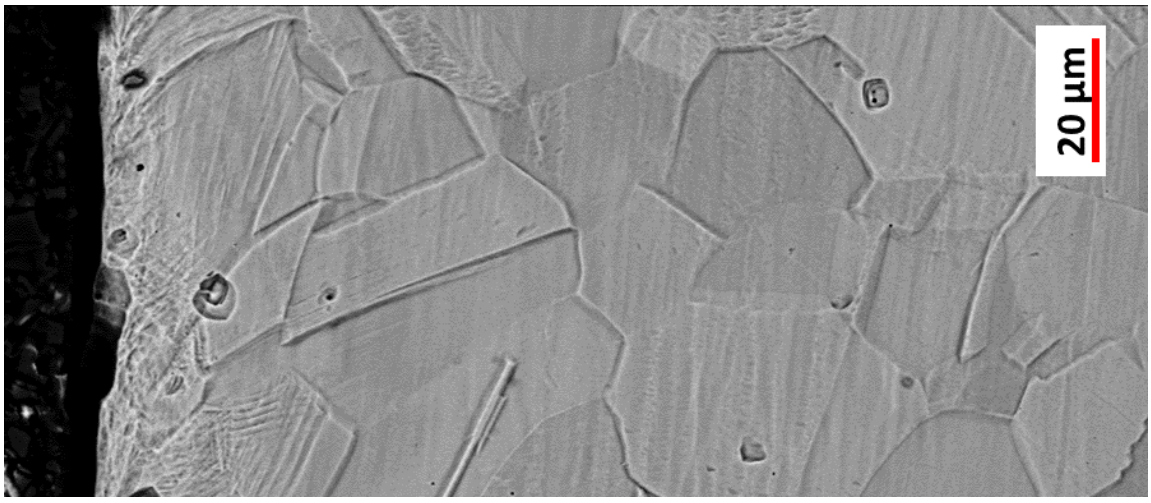


***Fig 3. SEM image showing etched cross-sectional microstructure of machined SS304L.***

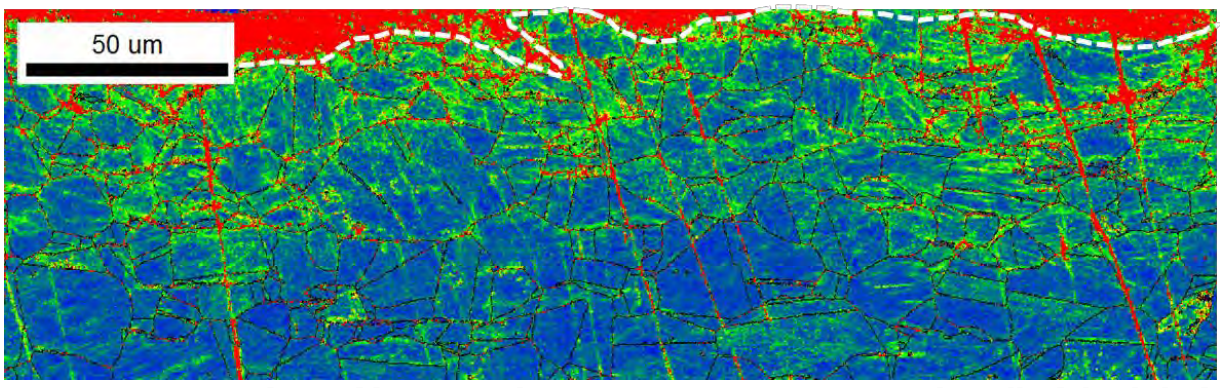


***Fig 4. KAM maps obtained by EBSD showing misorientations across the colloidal polished cross-section of machined SS304L.***

Fig 5 shows the variation in hardness along the cross-section of the machined specimen. The highest hardness was 463 $HV_{10}$ at 9 µm from the surface, which was the minimum distance at which measurements could be accurately taken. Subsequently, a smooth transition to bulk hardness values (252 $HV_{10}$) was observed over a thickness of up to 350 µm from the surface. As evidenced from cross-sectional SEM and KAM maps (Fig. 3 and 4), the SPD layer varies nonuniformly up to 10 µm from the surface. Hence, hardness values in this region would be highest. The first 50 µm shows a significantly higher hardness (414 - 463 $HV_{10}$) than the bulk. This region is seen in the KAM map (FIG___) to have clear strain localisations, both within the grain (nearer to the surface) and at the grain boundaries (further down towards the bulk) and the extend of deformation (viz. misorientations) goes down inwards into the bulk.

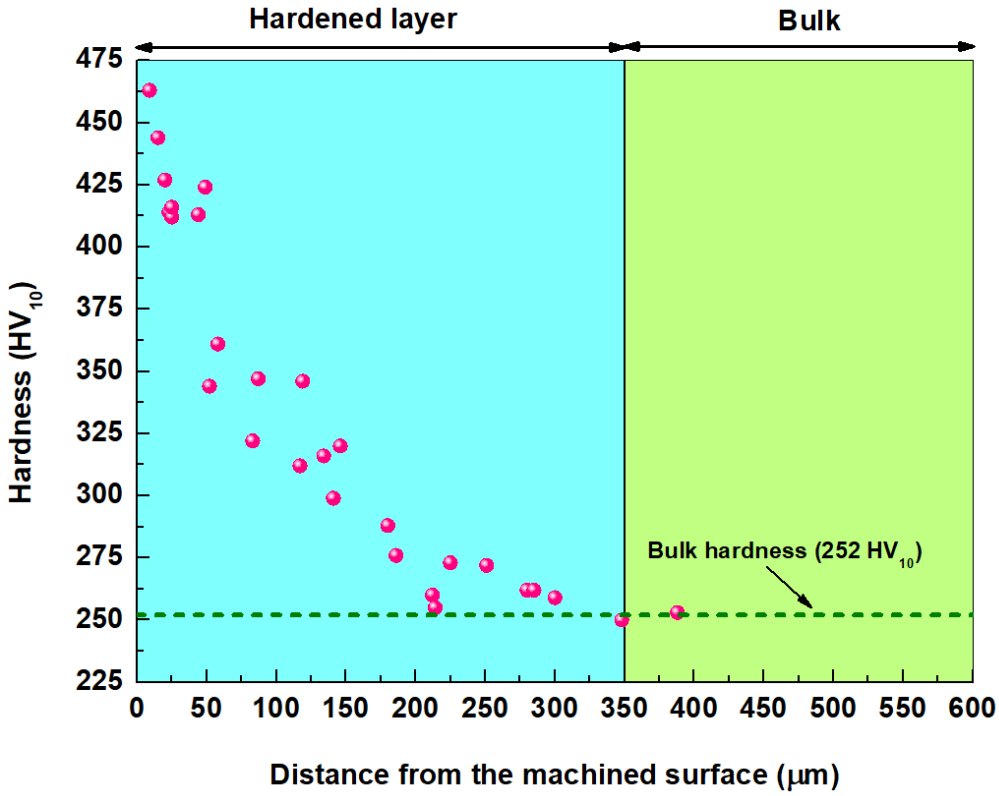


***Fig 5. Cross-sectional microhardness***

Post - oxidation characterisation : Set I

Fig 6 (a-d) presents stereomicroscopic images of oxidised coupons of machined SS304L (M15 - M60). All coupons were uniformly covered over all durations and no preferential oxidation could be readily observed.

Fig 7 (a-h) presents the SEM images showing oxide morphologies of films formed over machined surfaces (M15 - M60) post immersion for 15 d (Fig 7a,b), 30 d (Fig 7c,d), 45 d (Fig 7e,f) and 60 d (Fig 7g,h). The outer particles were tetrahedral with sharp edges, straight faces


**(a)** **(b)** **(c)** **(d)**

***Fig 6. Stereomicroscopic images of machined coupons exposed for 15 days (a), 30 days (b), 45 days (c) and 60 days (d) in high temperature DM water (300 ºC, 89 bar).***

and varied in size and distribution (Fig 7a-h). Numerous outer crystallites could be seen on the M15 surface prior to ultrasonic cleaning (Fig 7a), the density of which reduced significantly post ultrasonic cleaning (Fig 7b). A compact inner oxide scale becomes clearly visible post ultrasonic cleaning for all samples (Fig 7b,d,f,h) where loose outer crystallites have fallen off. However, the inner oxide is also prominent before ultrasonic cleaning for M45 (Fig 7e) and M60 (Fig 7g), where number of outer crystallites are low. For both M15 (Fig 7a) and M30 (Fig 7c), surface chips were still visible after exposure and outer crystals were seen to preferentially form under and around them. No such artefacts are visible on the M45 (Fig 7e) and M60 (Fig 7g) samples.

Fig 8 (a-d) plots the particle size distribution of the outer oxides (as calculated from SEM images) for M15 – M60 before and after ultrasonic cleaning. Particle size ranges for M15 – M60 are indicated in table 1. Number of faceted particles decrease (Fig 8a-d) post ultrasonic cleaning indicating that the bigger particles fell off - either due to weight or due to non-adherence (as also evident from the SEM images (Fig 7 a-h)). Number of particles also decrease with immersion time where M45 and M60 show lesser number of particles as compared to M15 and M30 samples both before and after ultrasonic cleaning. There is no clear trend in the maximum particle sizes.

Fig 9 shows the variation in specific weight change in M15 – M60 with time of exposure. The specific weight changes before and after ultrasonic cleaning follow the same trend. Initially, the M15 reports a small positive change in specific weight (1.50 $\mu g/cm^2$) before ultrasonication. Post ultrasonic cleaning, a negative specific weight change is reported by M15 ( -8.65 $\mu g/cm^2$). This may be attributed to the loss of loose outer oxide particles (Fig 7a,b, Fig 8a). Subsequently, all samples showed a weight loss with increasing duration of exposure (M30 – M60). However, the effect of ultrasonic cleaning is reduced as specific weights before and after cleaning remained nearly the same for M45 and M60. As shown in Fig 7 and 8, the number of outer oxides decrease with exposure time and are progressively more adherent, once formed. Hence, ultrasonic cleaning does not lead to significant change in specific weights. The negative weight change for SS samples exposed to high temperature phenomenon is an interesting observation and needs further exploration.

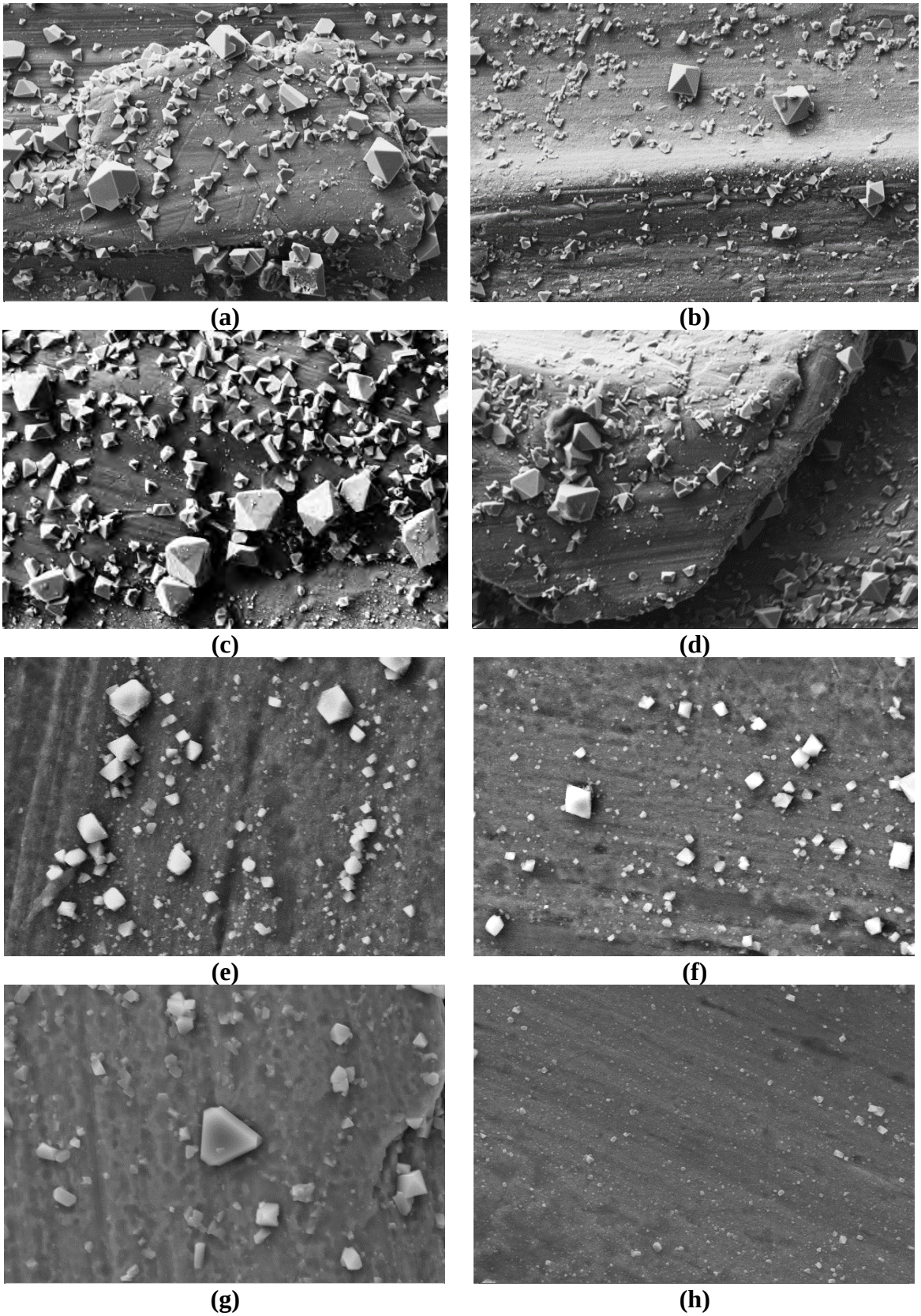


***Fig 7. SEM images of machined coupons exposed for 15 days (a,b), 30 days (c,d), 45 days (e,f) and 60 days (g,h) in high temperature DM water (300 ºC, 89 bar). Images a, c, e and g are taken before ultrasonic cleaning and b, d, f, and h are taken after ultrasonic cleaning of the oxidised coupons.***

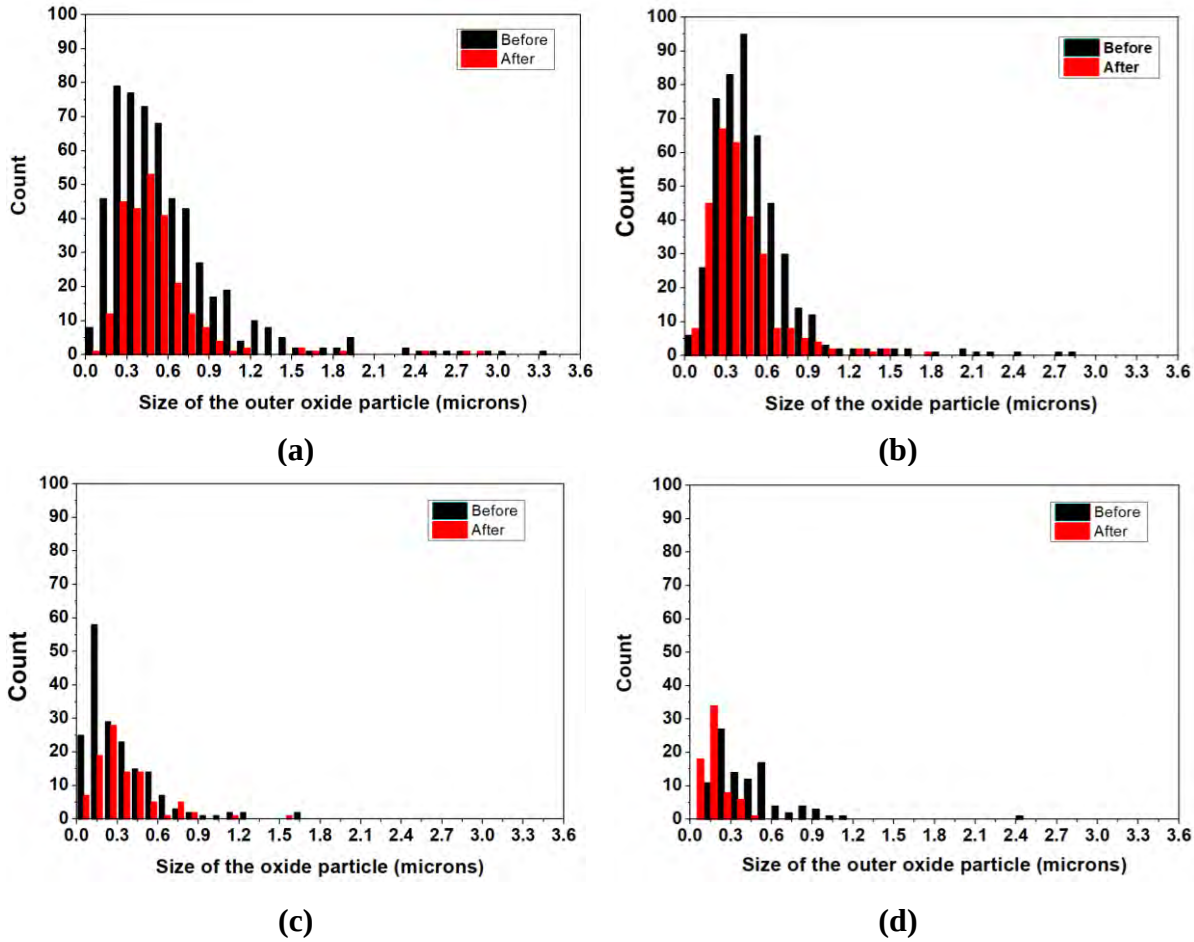


***Fig 8. Outer particle size distribution for machined coupons exposed to high temperature DM water for 15 d (a), 30 d (b), 45 d (c) and 60 d (d) - before and after ultrasonic cleaning.***

| | M15 | M30 | M45 | M60 |
|---|---|---|---|---|
| **Before ultrasonic cleaning** | 0.041 – 3.359 | 0.068 – 2.881 | 0.014 – 1.683 | 0.103 – 2.490 |
| **After ultrasonic cleaning** | 0.081 – 2.881 | 0.041 – 1.72 | 0.04 – 1.501 | 0.029 – 0.416 |

***Table 2. Histograms showing outer particle size ranges for machined SS304L coupons exposed to high temperature DM water - before and after ultrasonic cleaning.***

Fig 10 shows the variation in atomic wt.% of elements (Fe, Cr and Ni) at the I/O oxide interface formed over machined surfaces. In the race between iron, chromium and nickel for oxidation, chromium having the highest oxygen affinity, forms the first oxides which eventually constitute the inner, compact layer. Iron, having the highest diffusivity amidst the three, diffuses across this layer to the oxide/solution interface and forms the outer oxide. Nickel is retained at the metal/oxide surface and an apparent nickel enrichment is observed [18,19]. In the present case, chromium concentration at the inner/outer oxide interface is seen to increase progressively with time up till 45 days of immersion, beyond which it saturates. Iron concentration also decrease from 59 at. % for M15 to 53 at. % for M60 with time. Interestingly, nickel also shows an almost linear increase in concentration at the inner/outer oxide interface with exposure duration.

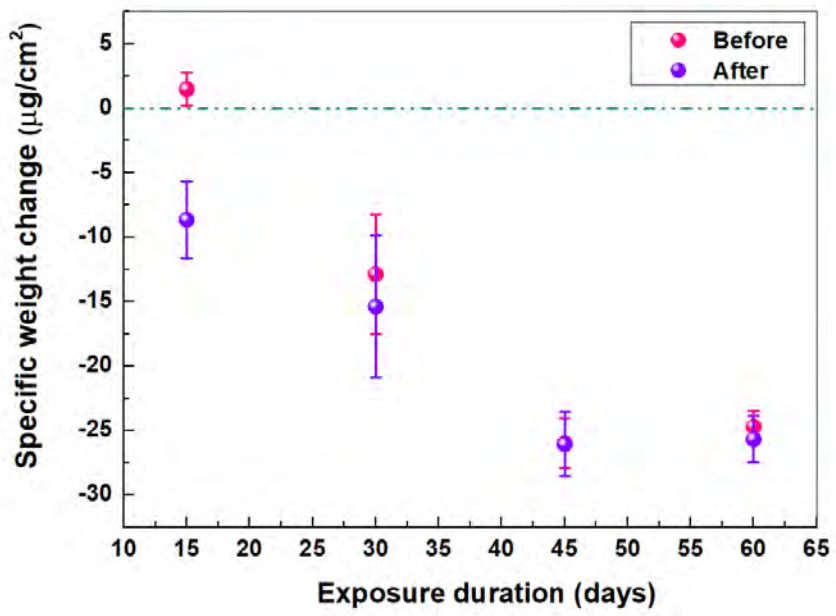


*Fig 9. Change in specific weights of machined SS304L coupons exposed to high temperature DM water for different durations - before and after ultrasonic cleaning.*

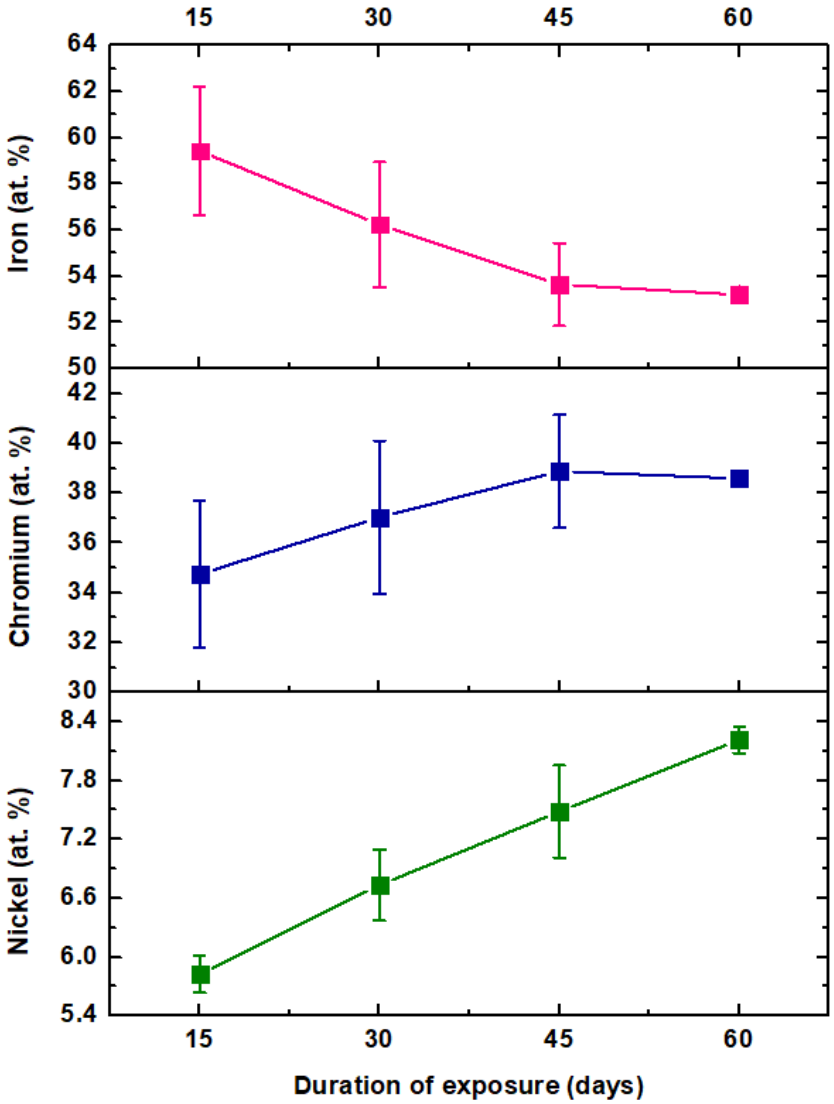


*Fig 10. GDOES results showing the variation in atomic wt.% of elements (Fe, Cr and Ni) at the inner/outer oxide interface as a function of exposure duration for oxides formed over machined surfaces.*

Post-exposure characterisation: Set II

**Fig 11 (a-d)** presents stereomicroscopic images of oxidised coupons of MC, 600, DP and EP specimen. It was evident that oxide formation was more aggressive in case of the first three as compared to the EP specimen.

**(a) (b) (c) (d)**

***Fig 11. Stereomicroscopic images of machined (MC) (a), #600 grit polished (600) (b), diamond polished (DP) (c) and electropolished (EP) (d) coupons exposed for 15 days in high temperature DM water (300 ºC, 89 bar).***

Fig 12 (a-h) presents the SEM images showing oxide morphologies of films formed over machined (Fig 12a,b), #600 grit polished (Fig 12c,d), Diamond polished (Fig 12e,f) and electropolished (Fig 12g,h) surfaces. Numerous loose outer oxide particles are observed over the MC specimen before ultrasonic cleaning (Fig 12 a) which fall off after cleaning (Fig 11b). the outer oxides formed over 600 (Fig 12 c) and DP (Fig 12 g) specimen are more adherent to the surface and remain marginally altered after cleaning (Fig d and h). The EP sample showed hardly any particles and the compact inner oxide could be clearly seen both before (Fig 12e) and after ultrasonic cleaning (Fig 12f). It was evident that surface hardened layer present as a result of surface working (machining and mechanical grinding) expedited the oxide film formation process. The electropolished specimen had had its deformed layer removed prior to exposure and hence, oxidation was slower. This kind of behaviour has also been previously reported. [13-15,18,20]. Further investigation into the electrochemical stability and elemental compositions of these films need to be carried out.

## Conclusion

Machining resulted in a deformed layer with a severely plastically deformed surface layer, followed by a sub-surface region of high strains. This deformed layer was observed to alter the oxide morphologies formed on SS with different surface states (600 grit polished, diamond polished and electropolished) after exposure to high temperature DM water. The machined coupons were exposed for up to 60 days. Numerous loose outer oxide particles were formed during the initial 30 days on the machined surface, which fell off after ultrasonic cleaning. Surface chips were visible on the machined surface after 15 and 30 days. Large outer oxides could be seen to form in the nooks and crannies around these chips and on the machined peaks. Beyond 30 days, they were fully consumed and were not visible on the 45 day coupons. GDOES results showed increasing chromium content in the inner oxide up to 45 days, after which it saturates. Further investigation is underway.

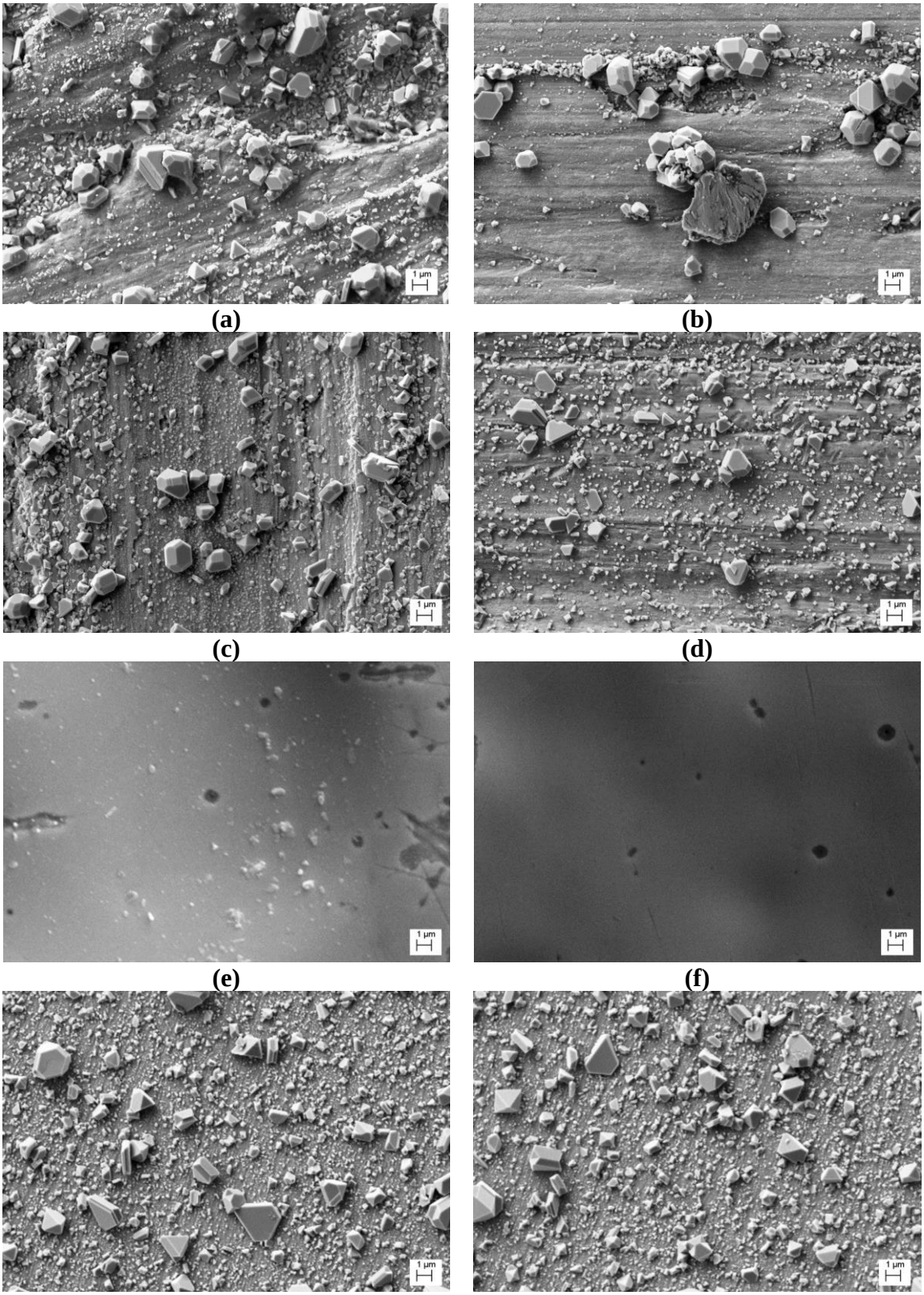

**(a)** **(b)**

**(c)** **(d)**

**(e)** **(f)**

**(g)** **(h)**

***SEM images of Machined (a,b), #600 grit polished (c,d), Electropolished (e,f) and Diamond polished (g,h) samples post high temperature oxidation in DM water (300 ºC, 89 bar). Images a, c, e and g are taken before ultrasonic cleaning and b, d, f, and h are taken after ultrasonic cleaning of the oxidised coupons.***

References


1) M. Fox, Journal of Materials for Energy Systems (1979) 3–13.
2) P.M. Scott, Corrosion Science, **25** (1985) 583.
3) J.R. Weeks, B. Vyas and H.S. Issacs, Corrosion Science, **25** (1985) 757.
4) P. M. Scott, Nuclear Materials, **211** (1994) 101.
5) R.M. Horn, G.M. Gordon, F.P. Ford and Cowan R.L., Nuclear Engineering and Design, **174** (1997) 313.
6) O. Wachter and G. Brümmer, Nuclear Engineering and Design, **168** (1997) 35.
7) P.L. Andresen, Corrosion **69** (2013) 1024.
8) S. Ghosh and V. Kain, Nuclear Materials, **403** (2010) 62.
9) S. Ghosh, V.P.S. Rana, V. Kain, V. Mittal and S.K. Baveja, Materials and Design **32** (2011) 3823.
10) G. Hinds, L. Wickstro, K. Ingard, and A. Turnbull, Corrosion Science, **71** (2013) 43.
11) W. Zhang, F. Kewei, H. Yujin, S. Wang and S. Wang, Corrosion Science, **108** (2016) 173.
12) X. Zhong, S.C. Bali and T. Shoji, Corrosion Science, **115** (2017) 106.
13) L. Chang, M. Grace Burke and F. Scenini, Corrosion Science **138** (2018) 54.
14) L. Chang, L. Volpe, Y.L. Wang, M. Grace Burke, A. Maurotto, D. Tice, S. Lozano-Perez and F. Scenini, Acta Materialia **165** (2019) 203.
15) L. Chang, M. Grace Burke and F. Scenini, Scripta Materialia **164** (2019) 1.
16) S.G. Acharyya, A. Khandelwal, V. Kain, A. Kumar and I. Samajdar, Materials Characterisation **72** (2012) 68.
17) K.B. Fisher, B.D. Miller, E.C. Johns and E.A. Marquis, Corrosion Science **141** (2018) 88.
18) S. Wang, Y. Hu, K. Fang, W. Zhang and X. Wang, Corrosion Science, **126** (2017) 104.
19) S. Ghosh, M. K. Kumar and V. Kain, Applied Surface Science, **264** (2013) 312.
20) S.E Ziemniak and M. Hanson, Corrosion Science, **44** (2002) 2209.
21) L. Jinlong, T. Liang and H. Luo, Nuclear Engineering and Design, **309** (2016) 1.
22) ASTM A262–15, 2015, Standard Practices for Detecting Susceptibility to Intergranular Attack in Austenitic Stainless Steels.
23) ASTM E112–13, 2013, Standard Test Methods for Determining Average Grain Size.
24) ASTM Standard G108–94, 2015, Standard Test Method for Electrochemical Reactivation (EPR) for Detecting Sensitization of AISI Type 304 and 304L Stainless Steels.
25) A. Das, S. Tarafder, S. Sivaprasad and D. Chakrabarti, Materials Science & Engineering A, **754** (2019) 348.
26) M. N. Gussev and K. J. Leonard, Journal of Nuclear Materials, **517** (2019) 45.
27) ASTM G2 / G2M – 19, 2019, Standard Test Method for Corrosion Testing of Products of Zirconium, Hafnium, and Their Alloys in Water at 680°F (360°C) or in Steam at 750°F (400°C).
28) A. Turnbull, K. Mingard, J.D. Lord, R. Roebuck, D.R. Tice, K.J. Mottershead and N.D. Fairweather, Corrosion Science, **53** (2011) 3398.